Dyes and Pigments 123 (2015) 100–111

Contents lists available at ScienceDirect

Dyes and Pigments

journal homepage: www.elsevier.com/locate/dyepig

Synthesis and characterization of alkoxyphenylthiophene substituted benzodithiophene-based 2D conjugated polymers for organic electronics applications

Kakaraparthi Kranthiraja [a], Kumarasamy Gunasekar [a], Nallan Chakravarthi [a], Myungkwan Song [b, **], Jong Hun Moon [c], Jin Yong Lee [c], In-Nam Kang [d], Sung-Ho Jin [a, *]

[a] Department of Chemistry Education, Graduate Department of Chemical Materials, BK 21 PLUS Team for Advanced Chemical Materials, and Institute for Plastic Information and Energy Materials, Pusan National University, Busan 609-735, Republic of Korea
[b] Surface Technology Division, Korea Institute of Materials Science, Changwon 641-831, Republic of Korea
[c] Department of Chemistry, Sungkyunkwan University, Suwon 440-746, Republic of Korea
[d] Department of Chemistry, The Catholic University of Korea, Bucheon, Republic of Korea

ARTICLE INFO

Article history:
Received 19 March 2015
Received in revised form
24 July 2015
Accepted 25 July 2015
Available online 1 August 2015

Keywords:
Low band gap polymers
Non-covalent interactions
Planar backbone
Polymer solar cells
Polymer field effect transistors
Side chain

ABSTRACT

In order to establish the correlation between intramolecular non-covalent interactions in the polymer backbone and the position/nature of alkoxy side chains in electron rich unit, two new series of low band gap polymers (**P1**–**P4**; **P5**–**P8**) were synthesized. We observed significant changes in photophysical properties upon changing the position and nature of the alkoxy side chain with respect to their intramolecular non-covalent interactions in the backbone, which are reflected in their field-effect transistors mobilities and photovoltaic properties. The Uv–Vis spectra of polymers containing a thieno[3,4-*c*]pyrrole-4,6-dione unit shows a vibronic shoulder, and the intensity of vibronic shoulder varies upon changing the position and nature of alkoxy side chain, in contrast, this type of absorption shoulder was not observed in polymer series containing a benzo[*c*][1,2,5]-thiadiazole moiety. In the thieno[3,4-*c*] pyrrole-4,6-dione series, a maximum power conversion efficiency of 4.19% with an open-circuit voltage of 0.91 V was noted. The power conversion efficiency of a benzo[*c*][1,2,5]-thiadiazole containing polymers was improved upon addition of 1,8-diiodooctane with maximum of 5.26% being recorded for polymer solar cells.

1. Introduction

Donor–acceptor (D–A) conjugated polymers have received great amount of interest in optoelectronics such as polymer solar cells, and polymer field effect transistors due to their advantage over their counterparts, (inorganic silicon materials), such as low cost, light weight, flexibility, and also possibility of large scale roll-to-roll processing of printed electronics [1]. Until today a huge number of D–A conjugated polymers have been designed and synthesized to improve the device performance of polymer solar cells and polymer filed effect transistors. But, the studies are mainly focused on the design of various types of conjugated materials and graft them with different alkyl chains [2]. In order to improve the device performance of polymer solar cells or polymer field effect transistors further it is crucial to study structure property relationships of conjugated polymers, such as side chain engineering, planarity of backbone and their effect on morphology which can strongly influence the performance of devices [3]. Recently few research groups have studied all the above properties and analyzed their effect on device performances. Particularly, the device performance, mainly depending on the planarity of the backbone of conjugated polymers [4,5].

In order to improve the planarity of backbone, many possible ways have been anticipated, such as synthesizing highly fused conjugated aromatic ring system, introduction of conjugated π-spacers between the electron rich and deficient units and the introduction of either planar aromatic electron rich or electron deficient units [6–8]. In some rare cases, the nature of the alkyl chain either on the electron rich unit or electron deficient unit has

* Corresponding author.
** Corresponding author.
E-mail addresses: smk1017@kims.re.kr (M. Song), shjin@pusan.ac.kr (S.-H. Jin).

http://dx.doi.org/10.1016/j.dyepig.2015.07.032
0143-7208/

also played a role on the planarity of the polymer backbone [9]. In recent times another way of improving the planarity of the backbone has become interesting, i.e. the intramolecular non-covalent interactions between the electron rich and electron deficient units of conjugated polymers, which can forcefully make the backbone planar [10]. It has been proven that these intramolecular non-covalent interactions greatly influence the bulk properties of conjugated polymers such as high mobility, better optical properties and suitable energy levels. These factors greatly influence the performance of polymer solar cells and polymer filed effect transistors in many cases [11]. According to the previous reports, the side chains grafted on the polymer backbone not only induce the solubility but also can modulate the morphology of the active layer when it blends with phenyl-C_{71}-butyric acid methyl ester ($PC_{71}BM$) as an acceptor in bulk hetero junction polymer solar cells [12]. To this end, we attempt to investigate the correlation between intramolecular non-covalent interactions in the backbone and the nature/position of alkyl chains on an electron rich unit of conjugated polymers to improve the planarity of the backbone.

Here, we have synthesized two series of conjugated polymers **P1**–**P4** and **P5**–**P8** containing the alkoxyphenylthiophene (APTh) linked benzodithiophene (BDT) as an electron rich and 1,3-di(2-bromothien-5-yl)-5-(2-ethylhexyl)thieno[3,4-*c*]pyrrole-4,6-dione (TPD) and [5,6-bis(octyloxy)-4,7-di(thiophen-2-yl)benzo[*c*][1,2,5]thiadiazole] (BT) as an electron deficient units as shown Scheme 1, respectively. We have analyzed the influence of nature (ethylhexyl to hexyldecyl) and position para (*p*) to meta (*m*) of the alkyl chain in APTh on the planarity of backbone with respect to their intramolecular non-covalent interactions. The intramolecular non-covalent interactions between the carbonyl oxygen and thiophene sulfur is stronger than the alkoxy oxygen and thiophene sulfur [13]. As we expected, there are significant differences in its photophysical, photovoltaic and transistor characteristics between the two series as well as within the series of polymers. The alkoxy side chains in APTh of all the polymers will be represented as follwos: *p*-ethylhexyloxyphenylthiophene (*p*-EHPTh), *p*-hexyldecyloxyphenylthiophene (*p*-HDPTh) and *m*-ethylhexyloxyphenylthiophene (*m*-EHPTh), *m*-hexyldecyloxyphenylthiophene (*m*-HDPTh), respectively.

2. Experimental

2.1. Materials and characterization

All chemicals and reagents were purchased from Sigma–Aldrich Chemical Co. Ltd, TCI, and Alfa Aesar, and were used without further purification. ^1H and ^{13}C NMR spectra were recorded on a Varian Mercury Plus 300 MHz, 600 MHz spectrometers in $CDCl_3$ using tetramethylsilane (TMS) as an internal standard. The FTIR spectra were measured using a JASCO FTIR spectrometer. The Uv–Vis absorption spectra were recorded on a JASCO V-570 spectrophotometer at room temperature. TGA was carried out on a Mettler Toledo TGA/SDTA 851e under N_2 atmosphere at a heating rate of 10 °C/min. Polymerization was conducted in CEM focused microwave TM synthesis system (CEM Discover-S). Weight average molecular weight (M_w), number average molecular weight (M_n), and polydispersity index (PDI) were determined against polystyrene as standard by GPC using PL gel 5 μm MLXED-C column on an Agilent 1100 series liquid chromatography system with tetrahydrofuran as an eluent. Cyclic voltammetry measurements were carried out in a 0.1 M solution of tetrabutylammonium tetrafluoroborate in anhydrous acetonitrile at a scan rate of 100 mV/s using CHI 600C potentiostat (CH Instruments); three electrode cell with platinum electrode as the working electrode, Ag/AgCl as the reference electrode and a platinum (Pt) wire as the counter electrode were used. Polymer thin films were coated on Pt electrode and dried before the experiment.

2.2. Polymer field effect transistors fabrication and characterization

Bottom contact geometry polymer filed effect transistors was fabricated to examine the charge-transport properties of polymers. The photoactive layers were deposited by spin coating a 5 mg/mL

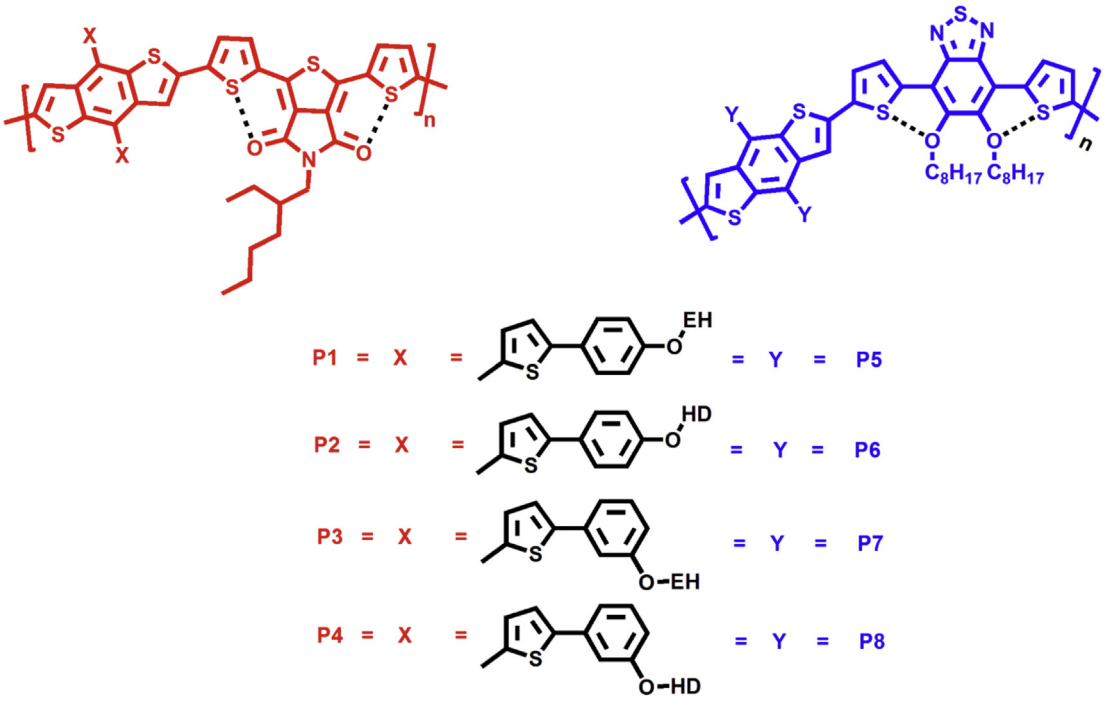

Scheme 1. Structures of polymers.

polymer solution in chloroform under a N_2 atmosphere onto n-octyltrichlorosilane, n-doped silicon wafer with a 300 nm thickness of SiO_2 dielectric layer. The devices were then annealed for 10 min at 140 °C in a glove box under N_2 atmosphere. The polymer filed effect transistors characteristics were determined under ambient conditions, and no precautions were taken to insulate the materials or devices from exposure to air, moisture, or light. The field effect mobility was calculated in the saturation regime by using the equation $I_{DS} = (\mu WC_i/2L)(V_G - V_T)^2$, where I_{DS} is the drain-source current, μ is the field effect mobility, W is the channel width (120 μm), L is the channel length (12 μm), C_i is the capacitance per unit area of the gate dielectric layer, and V_G is the gate voltage.

2.3. Fabrication and characterization of the bulk heterojunction polymer solar cells

The ITO and glass substrates that have been used for fabrication were ultrasonically cleaned with detergent, water, acetone, and isopropyl alcohol. Then, a 40 nm thick layer of PEDOT:PSS was coated on the electrodes by spin coating a solution of PEDOT:PSS diluted with isopropyl alcohol with the dilution ratio being 1:2 and annealed at 150 °C for 10 min in oven. A 90 ± 10 nm thick active layer of **P1**–**P8**:$PC_{71}BM$ was spin coated using a mixture of polymer:$PC_{71}BM$ (8 mg:16 mg) that was dissolved in 1 mL of chlorobenzene and further mixed with 1–3 vol% 1,8 diiodooctane (DIO). A 0.7 nm thickness of LiF and 100 nm thick Al cathode was deposited via evaporation on the active layer. The performances of the bulk heterojunction polymer solar cells were measured under simulated AM 1.5G illumination (100 mW/cm^2). The irradiance of the sunlight simulating illumination was calibrated using a standard Si photodiode detector fitted with a KG5 filter. The performance of the bulk heterojunction polymer solar cells were measured using calibrated air mass (AM) 1.5G solar simulator (Oriel® Sol3A™ Class AAA solar simulator, models 94043A) with a light intensity of 100 mW/cm^2 adjusted using a standard PV reference cell (2 cm × 2 cm monocrystalline silicon solar cell, calibrated at NREL, Colorado, USA) and a computer controlled Keithley 2400 source measure unit. The incident photon to current conversion efficiency spectrum was measured using Oriel® IQE-200™ equipped with a 250 W quartz tungsten halogen lamp as the light source and a monochromator, an optical chopper, a lock-in amplifier, and a calibrated silicon photodetector. The thickness of the thin films was measured using a KLA Tencor Alpha-step IQ surface profilometer with an accuracy of ±1 nm. AFM images were acquired with a XE-100 (park system corp.) in tapping mode.

2.4. Synthesis of compounds ***1***–***4***

The compounds **1**–**4** were synthesized by applying the similar procedure. The representative procedure for compound **1** is as follows: 4-bromophenyl-2-ethylhexyl ether (6 g, 21 mmol) and 2-tributylstannylthiophene (10 mL, 31.5 mmol) were added to dry toluene (30 mL) and purged with N_2 for 20 min and then $Pd(PPh_3)_4$ (1.2 g, 1.05 mmol) was added to the reaction mixture and refluxed overnight. After completion of reaction, the reaction mixture was cooled to room temperature and the solvent was removed. Crude product was extracted with methylene chloride (2 × 100 mL), washed with water, brine solution, and dried over anhydrous $MgSO_4$. The resulted crude was purified by column chromatography on silica gel with hexane as an eluent.

2.4.1. Synthesis of 2-(4-(2-ethylhexyloxy)phenyl)thiophene (colorless oil ***1***, yield 66%)

^{1}H NMR (300 MHz, $CDCl_3$): δ (ppm) 7.51 (d, J = 6 Hz, 2H), 7.19–7.25 (m, 2H), 7.02–7.08 (m, 1H), 6.90 (d, J = 9 Hz, 2H), 3.85 (d, J = 6 Hz, 2H), 1.7 (m, 1H), 1.33–1.55 (m, 8H), 0.9 (m, 6H). ^{13}C NMR (300 MHz, $CDCl_3$): δ (ppm) 159.33, 144.77, 128.13, 127.42, 127.30, 123.94, 122.22, 115.15, 70.90, 39.67, 30.82, 29.37, 24.15, 23.32, 14.35, 11.38. HRMS (EI$^+$, m/z) [M$^+$] calcd for $C_{18}H_{24}OS$ 288.15; found, 288.12.

2.4.2. Synthesis of 2-(4-(2-hexyldecyloxy)phenyl)thiophene (colorless oil ***2***, yield 68%)

^{1}H NMR (300 MHz, $CDCl_3$): δ (ppm) 7.46–7.58 (m, 2H), 7.16–7.22 (m, 2H), 7.02–7.08 (m, 1H), 6.86–6.94 (m, 2H), 3.80–3.90 (m, 2H), 1.70–1.80 (m, 1H), 1.10–1.40 (m, 24H), 0.80–0.90 (m, 6H). ^{13}C NMR (300 MHz, $CDCl_3$): δ (ppm) 159.32, 144.76, 128.10, 127.40, 127.26, 123.91, 122.18, 115.14, 71.31, 38.22, 32.16, 32.11, 31.64, 30.27, 29.94, 29.84, 29.58, 28.52, 27.10, 27.08, 27.01, 22.92, 17.51, 14.34, 13.82. HRMS (EI$^+$, m/z) [M$^+$] calcd for $C_{26}H_{40}OS$ 400.28; found, 400.20.

2.4.3. Synthesis of 2-(3-(2-ethylhexyloxy)phenyl)thiophene (colorless oil ***3***, yield 70%)

^{1}H NMR (300 MHz, $CDCl_3$): δ (ppm) 7.27–7.31 (m, 3H), 7.14–7.20 (m, 2H), 7.05–7.09 (m, 1H), 6.81–6.84 (m, 1H), 3.84–3.90 (m, 2H), 1.58–1.75 (m, 1H), 1.33–1.53 (m, 8H), 0.91–0.97 (m, 6H). ^{13}C NMR (300 MHz, $CDCl_3$): δ (ppm) 160.24, 144.64, 135.89, 130.02, 128.10, 124.98, 124.98, 123.43, 118.54, 113.78, 112.57, 70.80, 39.67, 30.79, 29.34, 28.49, 26.97, 24.13, 23.27, 17.51, 14.28, 13.78, 11.35. HRMS (EI$^+$, m/z) [M$^+$] calcd for $C_{18}H_{24}OS$ 288.15; found, 288.14.

2.4.4. Synthesis of 2-(3-(2-hexyldecyloxy)phenyl)thiophene (colorless oil ***4***, yield 73%)

^{1}H NMR (300 MHz, $CDCl_3$): δ (ppm) 7.28–7.34 (m, 3H), 7.1–7.2 (m, 2H), 7.02–7.08 (m, 1H), 6.80–6.88 (m, 2H), 3.8–3.9 (m, 2H), 1.8 (m, 1H), 1.2–1.4 (m, 24), 0.8–0.95 (m, 6H). ^{13}C NMR (300 MHz, $CDCl_3$): δ (ppm) 160.06, 150.59, 144.67, 135.91, 130.02, 129.09, 128.10, 126.18, 124.95, 123.42, 123.27, 118.52, 113.79, 112.59, 108.61, 71.20, 38.28, 36.67, 32.18, 32.13, 28.54, 27.02, 22.94, 19.67, 17.74, 15.34, 13.82. HRMS (EI$^+$, m/z) [M$^+$] calcd for $C_{26}H_{40}OS$ 400.28; found, 400.24.

2.5. Synthesis of compound ***5***–***8***

The compounds **5**–**8** were synthesized by applying the similar procedure. The synthetic procedure for **5** is as follows: Compound **1** (2.59 g, 9 mmol) in dry tetrahydrofuran (25 mL), n-BuLi (3.6 mL, 9 mmol) was added dropwise at 0 °C, then reaction mixture was heated to 50 °C for 2 h and then 4,8-dihydrobenzo[1,2-b:4,5-b] dithiophen-4,8-dione (1 g, 4.53 mmol) was added to reaction mixture at same temperature and then continued the heating for 2 h and the reaction mixture was cooled to room temperature and then $SnCl_2 \cdot 2H_2O$ (4.08 g, 18 mmol) in 10 mL (H_2O:HCl 7:3 v/v) was added to reaction mixture and then stirred for overnight. The reaction mixture was then poured into cold water and extracted with diethyl ether and dried over anhydrous $MgSO_4$ and then evaporated the organic layer and the resulted crude product was purified by column chromatography on silica gel with (hexane: methylene chloride 9:1 v/v) to furnish a yellow colored solid.

2.5.1. Synthesis of 4,8-Bis(2-(4-(2-ethylhexyloxy)phenyl)-5-thienyl) benzo[1,2-b:4,5-b′]dithiophene (yellow color solid ***5***, 28.9%). mp 132–134 °C

^{1}H NMR (300 MHz, $CDCl_3$): δ (ppm) 7.72 (d, J = 6 Hz, 2H), 7.61 (d, J = 6 Hz, 4H), 7.44–7.50 (m, 4H), 7.32 (d, J = 3 Hz, 2H), 6.94–6.97 (m, 4H), 3.88–3.90 (m, 4H), 1.72–1.77 (m, 2H), 1.36–1.54 (m, 16H), 0.93–0.98 (m, 12H). ^{13}C NMR (300 MHz, $CDCl_3$): δ (ppm) 159.57, 145.69, 139.31, 138.08, 136.83, 129.311, 127.922, 127.36, 126.91, 124.09, 123.61, 122.45, 115.25, 70.95, 39.64, 30.78, 29.33, 24.12,

23.27, 14.29, 11.34. HRMS (EI$^+$, m/z) [M$^+$] calcd for $C_{46}H_{50}O_2S_4$ 762.27; found, 762.25.

*2.5.2. Synthesis of 4,8-Bis(2-(4-(2-hexyldecyloxy)phenyl)-5-thienyl)benzo[1,2-b:4,5-b′]dithiophene (yellow color solid **6**, 40%). mp 99–101 °C*

^{1}H NMR (300 MHz, $CDCl_3$): δ (ppm) 7.71 (d, J = 5.7 Hz, 2H), 7.61 (d, J = 8.4 Hz, 4H), 7.44–7.52 (m, 4H), 7.33–7.34 (m, 2H), 6.90–6.98 (m, 4H), 3.9 (m, 4H), 1.9 (m, 2H), 1.1–1.4 (m, 48H), 0.9 (m, 12H). ^{13}C NMR (300 MHz, $CDCl_3$): δ (ppm) 159. 58, 145.70, 139.31, 138.08, 136.82, 129.31, 127.92, 127.92, 127.34, 126.90, 124.09, 123.62, 122.44, 115.25, 71.37, 38.22, 32.14, 31.63, 27.08, 22.90, 14.32. HRMS (EI$^+$, m/z) [M$^+$] calcd for $C_{62}H_{82}O_2S_4$ 986.52; found, 986.50.

*2.5.3. Synthesis of 4,8-Bis(2-(3-(2-ethylhexyloxy)phenyl)-5-thienyl)benzo[1,2-b:4,5-b′]dithiophene (yellow solid **7**, yield: 26%). mp 100–103 °C*

^{1}H NMR (300 MHz, $CDCl_3$): δ (ppm) 7.70 (d, J = 6 Hz, 2H), 7.44–7.51 (m, 6H), 7.28–7.33 (m, 6H), 6.82–6.90 (m, 2H), 3.90–3.92 (m, 4H), 1.74–1.80 (m, 2H), 1.35–1.51 (m, 16H), 0.91–0.99 (m, 12H). ^{13}C NMR (300 MHz, $CDCl_3$): δ (ppm) 160.13, 145.56, 139.36, 136.85, 135.56, 130.15, 129.30, 128.04, 124.06, 123.06, 118.47, 114.16, 112.49, 70.89, 39.70, 31.07, 29.35, 24.15, 23.27, 14.28, 11.36. HRMS (EI$^+$, m/z) [M$^+$] calcd for $C_{46}H_{50}O_2S_4$ 762.27; found, 762.22.

*2.5.4. Synthesis of 4,8-Bis(2-(3-(2-hexyldecyloxy)phenyl)-5-thienyl)benzo[1,2-b:4,5-b′]dithiophene (yellow oil **8**, 40%)*

^{1}H NMR (300 MHz, $CDCl_3$): δ (ppm) 7.68–7.74 (m, 2H), 7.42–7.52 (m, 4H), 7.20–7.36 (m, 8H), 6.82–6.90 (m, 2H), 3.89–3.91 (m, 4H), 1.81 (m, 2H), 1.29–1.54 (m, 48H), 0.9 (m, 12H). ^{13}C NMR (300 MHz, $CDCl_3$): 160.14, 145.57, 139.36, 139.18, 136.85, 135.56, 130.16, 129.31, 128.05, 126.12, 124.06, 123.77, 123.55, 118.46, 114.17, 112.49, 71.28, 38.27, 32.10, 31.66, 30.26, 29.93, 29.82, 29.56, 27.10, 22.90, 12.32. HRMS (EI$^+$, m/z) [M$^+$] calcd for $C_{62}H_{82}O_2S_4$ 986.52; found, 986.53.

*2.6. Synthesis of **D1**–**D4***

Monomers **D1**–**D4** was synthesized by applying the similar procedure. The synthetic procedure for **D1** is as follows: A solution of compound **5** (0.6 g, 0.78 mmol) in dry tetrahydrofuran (20 mL) at −78 °C under N_2 atmosphere, *tert*-BuLi (0.92 mL) was added dropwise stirred for 30 min at same temperature and trimethyltin chloride (0.312 g, 1.57 mmol) was added at one shot to reaction mixture at −78 °C and then stirred the reaction mixture at room temperature for overnight. Aqueous sodium carbonate solution was added slowly to reaction mixture and then extracted with diethyl ether and dried over anhydrous $MgSO_4$ to get yellow solid upon recrystallization with ethanol.

*2.6.1. Synthesis of 2,6-Bis(trimethyltin)-4,8-bis(2-(4-(2-ethylhexyloxy)phenyl)-5-thienyl)benzo[1,2-b:4,5′]dithiophene (yellow solid **D1**, 70%). mp 179–181 °C*

^{1}H NMR (300 MHz, $CDCl_3$): δ (ppm) 7.75 (s, 2H), 7.63 (d, J = 9 Hz, 4H), 7.46 (d, J = 3 Hz, 2H), 7.35 (d, J = 3 Hz, 2H), 6.95–7.01 (m, 4H), 3.89–3.94 (m, 4H), 1.74–1.78 (m, 2H), 1.36–1.52 (m, 16H), 0.93–0.98 (m, 12H), 0.31–0.54 (m, 18H). ^{13}C NMR (300 MHz, $CDCl_3$): δ (ppm) 159.50, 145.35, 143.62, 142.95, 138.95, 137.66, 131.28, 129.19, 127.36, 127.10, 122.44, 115.24, 70.96, 39.65, 30.79, 29.34, 24.13, 23.26, 14.29, 11.35. FTIR (KBr, cm^{-1}) 2964, 2918, 2862, 1601. HRMS (EI$^+$, m/z) [M$^+$] calcd for $C_{52}H_{66}O_2S_4Sn_2$ 1090.20; found, 1090.18.

*2.6.2. Synthesis of 2,6-Bis(trimethyltin)-4,8-bis(2-(4-(2-hexyldecyloxy)phenyl)-5-thienyl)benzo[1,2-b:4,5-b′]dithiophene (yellow oil **D2**, 75%)*

^{1}H NMR (300 MHz, $CDCl_3$): δ (ppm) 7.82 (s, 2H), 7.66–7.69 (m, 4H), 7.51–7.53 (m, 2H), 7.38–7.39 (m, 2H), 6.98–7.01 (m, 4H), 3.91–3.93 (m, 4H), 1.85 (m, 2H), 0.86–0.89 (m, 48H), 0.37–0.55 (m, 18H). ^{13}C NMR (300 MHz, $CDCl_3$): 159.55, 145.58, 143.68, 142.97, 138.98, 137.72, 131.34, 129.25, 127.39, 122.48, 115.29, 71.39, 38.27, 32.20, 30.31 29.62, 27.1422.97, 14.40. FTIR (KBr, cm^{-1}) 2956, 2928, 2847, 1607. HRMS (EI$^+$, m/z) [M$^+$] calcd for $C_{68}H_{98}O_2S_4Sn_2$ 1314.45; found, 1314.40.

*2.6.3. Synthesis of 2,6-Bis(trimethyltin)-4,8-bis(2-(3-(2-ethylhexyloxy)phenyl)-5-thienyl)benzo[1,2-b:4,5-b′]dithiophene (yellow solid **D3**, 64%). mp 131–133 °C*

^{1}H NMR (300 MHz, $CDCl_3$): δ (ppm) 7.73 (s, 2H), 7.31–7.48 (m, 10H), 6.84–6.90 (m, 2H), 3.92–3.94 (m, 4H), 1.74–1.80 (m, 2H), 1.34–1.53 (m, 16H), 0.92–0.99 (m, 12H), 0.32–0.42 (m, 18H). ^{13}C NMR (300 MHz, $CDCl_3$): δ (ppm) 160.12, 145.21, 143.66, 143.16, 140.05, 137.69, 135.75, 131.17, 130.13, 129.19, 123.76, 122.36, 118.52, 114.07, 112.51, 70.93, 39.69, 30.82, 29.34, 24.16, 23.27, 14.28, 11.35. FTIR (KBr, cm^{-1}) 2964, 2918, 2866, 1597. HRMS (EI$^+$, m/z) [M$^+$] calcd for $C_{52}H_{66}O_2S_4Sn_2$ 1090.20; found, 1090.19.

*2.6.4. Synthesis of 2,6-Bis(trimethyltin)-4,8-bis(2-(3-(2-hexyldecyloxy)phenyl)-5-thienyl)benzo[1,2-b:4,5-b′]dithiophene (yellow oil **D4**, 68%)*

^{1}H NMR (300 MHz, $CDCl_3$): δ (ppm) 7.73 (s, 2H), 7.48–7.50 (m, 4H), 7.31–7.46 (m, 6H), 3.91–3.95 (m, 2H), 1.83 (m, 2H), 1.08–1.48 (m, 48H), 0.69–0.88 (m, 12H),0.32–0.51 (m, 18H). ^{13}C NMR (300 MHz, $CDCl_3$): δ (ppm) 160.12, 145.56, 143.26, 143.15, 140.04, 139.57, 139.18, 138.26, 137.68, 136.85, 136.24, 135.73, 131.17, 130.14, 129.20, 128.07, 123.77, 122.36, 118.49, 114.06, 112.48. FTIR (KBr, cm^{-1}) 2965, 2929, 2865, 1593. HRMS (EI$^+$, m/z) [M$^+$] calcd for $C_{68}H_{98}O_2S_4Sn_2$ 1314.45; found, 1314.42.

2.7. General polymerization procedure

All the polymers were synthesized by applying microwave-assisted Stille polymerization. The representative procedure for the synthesis of polymer **P1** is as follows: To a 10 mL microwave tube, compound **D1** (300 mg, 0.275 mmol), and 1,3-di(2-bromothien-5-yl)-5-(2-ethylhexyl)thieno[3,4-*c*]pyrrole-4,6-dione (**A1**) (161 mg, 0.275 mmol), Pd_2 (dba)$_3$ (5.4 mg, 2 mol %), and (*o*-tol)$_3$P (16 mg, 16 mol %) were dissolved in anhydrous chlorobenzene, 5 mL). The reaction mixture was purged with N_2 for 15 min. The microwave tube was placed into the reactor and heated to 120 °C for 30 min. After cooling to room temperature reaction mixture was poured into methanol to obtain precipitate. The resulted precipitate was purified by soxhlet extraction method using methanol, hexane, acetone, and chloroform. The chloroform fraction was evaporated to get **P1**.

*Poly[4,8-bis(2-(4-(2-ethylhexyloxy)phenyl)-5-thienyl)benzo[1,2-b:4,5-b′]dithiophene-alt-1,3-di(2-bromothien-5-yl)-5-(2-ethylhexyl) thieno[3,4-c]pyrrole-4,6-dione] (**P1**, 58%). M_n* and PDI are 26,000 g/mol and 1.2. ^{1}H NMR (300 MHz, $CDCl_3$): δ (ppm) 7.5–7.68 (br, 4H), 7.19–7.39 (br, 10H), 6.92 (br, 4H), 3.87 (br, 4H) 3.53 (br, 2H) 1.76 (br, 3H), 1.25–1.55 (br, 16H), 0.85–0.95 (br, 18H). ^{13}C NMR (600 MHz, $CDCl_3$): δ (ppm) 127.17, 120.99, 114.85, 70.63, 39.42, 30.53, 29.68, 29.12, 26.03, 23.86, 23.07, 22.64, 14.09, 11.12. FTIR (KBr, cm^{-1}) 3430, 3071, 2927, 2847, 1751, 1681. Anal. Calcd for $C_{68}H_{69}NO_4S_7$: C, 68.71; H, 5.85; N, 1.18. Found C, 68.55; H, 6.06; N, 1.41.

*Poly[4,8-bis(2-(4-(2-hexyldecyloxy)phenyl)-5-thienyl)benzo[1,2-b:4,5-b′]dithiophene-alt-1,3-di(2-bromothien-5-yl)-5-(2-ethylhexyl) thieno[3,4-c]pyrrole-4,6-dione] (**P2**, 59%). M_n* and PDI are 27,000 g/

mol and 1.3. ^{1}H NMR (300 MHz, $CDCl_3$): δ (ppm) 7.60–7.77 (br, 4H), 7.25–7.27 (br, 10H), 6.94 (br, 4H), 3.87 (br, 4H), 3.52 (br, 2H), 1.76 (br, 3H), 1.31–0.56 (br, 48H), 0.89 (br, 18H). ^{13}C NMR (600 MHz, $CDCl_3$): δ (ppm) 38. 00, 31.91, 31.37, 29.69, 26.85, 22.68, 17.34, 14.11. FTIR (KBr, cm^{-1}) 3441, 3057, 2917, 2858, 1756, 1695. Anal. Calcd for $C_{84}H_{101}NO_4S_7$: C, 71.39; H, 7.20; N, 0.99. Found C, 71.74; H, 7.30; N, 1.28.

*Poly[4,8-bis(2-(3-(2-ethylhexyloxy)phenyl)-5-thienyl)benzo[1,2-b:4,5-b′]dithiophene-alt-1,3-di(2-bromothien-5-yl)-5-(2-ethylhexyl) thieno[3,4-c]pyrrole-4,6-dione] (**P3**, 64%).* M_n and PDI are 30,000 g/mol and 1.2. ^{1}H NMR (300 MHz, $CDCl_3$): δ (ppm) 7.19–7.47 (br, 10H), 6.88 (br, 8H), 3.9 (br, 4H), 3.49 (br, 2H), 1.9 (br, 3H), 1.35–1.54 (br, 24H), 0.93 (br, 18H). ^{13}C NMR (600 MHz, $CDCl_3$): δ (ppm) 162.34, 159.79, 145.12, 140.22, 139.28, 138.47, 137.95, 136.67, 135.27, 135.21, 132.10, 130.32, 129.84, 128.25, 127.56, 125.63, 123.75, 122.92, 119.51, 118.25, 113.76, 112.03, 76.78, 70.53, 42.52, 39.43, 38.09, 30.54, 29.10, 28.50, 23.87, 14.09, 11.15, 10.43. FTIR (KBr, cm^{-1}) 3446, 3057, 2917, 2847, 1756, 1691. Anal. Calcd for $C_{68}H_{69}NO_4S_7$: C, 68.71; H, 5.85; N, 1.18. Found C, 68.97; H, 6.15; N, 1.31.

*Poly[4,8-bis(2-(3-(2-hexyldecyloxy)phenyl)-5-thienyl)benzo[1,2-b:4,5-b′]dithiophene-alt-1,3-di(2-bromothien-5-yl)-5-(2-ethylhexyl) thieno[3,4-c]pyrrole-4,6-dione] (**P4**, 62%).* M_n and PDI are 28,000 g/mol and 1.2. ^{1}H NMR (300 MHz, $CDCl_3$): δ (ppm) 7.6–7.9 (br, 4H), 7.23–7.46 (br, 10H), 6.88 (br, 4H), 3.91 (br, 4H), 3.5 (br, 2H), 1.82 (br, 3H), 1.29–1.58 (br, 48H), 0.88 (br, 18H). ^{13}C NMR (600 MHz, $CDCl_3$): δ (ppm) 162.49, 159.82, 145.58, 139.56, 137.00, 136.31, 135.33, 132.61, 130.68, 129.83, 126.69, 123.78, 118.41, 113.91, 112.16, 71.03, 42.48, 38.08, 31.41, 30.49, 29.35, 23.78, 10.37. FTIR (KBr, cm^{-1}) 3437, 3077, 2917, 2847, 1751, 1691. Anal. Calcd for $C_{84}H_{101}NO_4S_7$. C, 71.39; H, 7.20; N, 0.99. Found C, 71.62; H, 7.49; N, 1.27.

*Poly[4,8-bis(2-(4-(2-ethylhexyloxy)phenyl)-5-thienyl)benzo[1,2-b:4,5-b′]dithiophene -alt-5,6-bis(octyloxy)-4,7-di(thiophen-2-yl) benzo[c][1,2,5]thiadiazole] (**P5**, 62%).* M_n and PDI are 33,000 and 1.2. ^{1}H NMR (300 MHz, $CDCl_3$): δ (ppm) 8.48 (br, 2H), 7.68–7.80 (br, 2H), 7.48–7.49 (br, 6H), 7.25–7.36 (br, 4H), 6.90 (br, 4H), 4.13 (br, 4H), 3.89 (br, 4H), 1.77–1.92 (br, 2H), 1.25–1.54 (br, 44H), 0.95 (br, 18H). ^{13}C NMR (600 MHz, $CDCl_3$): δ (ppm) 159.33, 150.15, 145.48, 138.52, 129.08, 128.10, 122.24, 114.99, 70.68, 39.41, 31.76, 30.54, 29.11, 25.91, 23.88, 22.68. 14.10, 11.14. FTIR (KBr, cm^{-1}) 3435, 3077, 2913, 2847, 1729, 1592. Anal. Calcd for $C_{76}H_{86}N_2O_4S_7$. C, 69.36; H, 6.59; N, 2.13; Found C, 69.97; H, 6.92; N, 2.31.

*Poly[4,8-bis(2-(4-(2-hexyldecyloxy)phenyl)-5-thienyl)benzo[1,2-b:4,5-b′]dithiophene-alt-5,6-bis(octyloxy)-4,7-di(thiophen-2-yl) benzo[c][1,2,5]thiadiazole] (**P6**, 62%).* M_n and PDI are 35,000 and 1.3. ^{1}H NMR (300 MHz, $CDCl_3$): δ (ppm) 8.44 (br, 2H), 7.36–7.63 (br, 8H), 7.25–7.36 (br, 4H), 6.89 (br, 4H), 4.13 (br, 4H), 3.87 (br, 4H), 1.81–1.91 (br, 2H), 1.28–1.53 (br, 76H), 0.90 (br, 18H). ^{13}C NMR (600 MHz, $CDCl_3$): δ (ppm) 159.37, 129.26, 127.09, 115.00, 71.11, 38.00, 31.91, 29.70, 26.87, 22.68, 14.12. FTIR (KBr, cm^{-1}) 3439, 3069, 2918, 2852, 1714, 1611. Anal. Calcd for $C_{92}H_{118}N_2O_4S_7$. C, 71.73; H, 7.72; N, 1.82. Found C, 72.02; H, 8.06; N, 1.78.

*Poly[4,8-bis(2-(3-(2-ethylhexyloxy)phenyl)-5-thienyl)benzo[1,2-b:4,5-b′]dithiophene -alt-5,6-bis(octyloxy)-4,7-di(thiophen-2-yl) benzo[c][1,2,5]thiadiazole] (**P7**, 52%).* M_n and PDI are 24,000 and 1.3. ^{1}H NMR (300 MHz, $CDCl_3$): δ (ppm) 8.48 (br, 2H), 7.68–7.83 (br, 2H), 7.48–7.49 (br, 6H), 7.25–7.43 (br, 4H), 6.90 (br, 4H), 4.14 (br, 4H), 3.92–3.94 (br, 4H), 1.77–1.92 (br, 2H), 1.25–1.54 (br, 44H), 0.82–0.98 (br, 18H). ^{13}C NMR (600 MHz, $CDCl_3$): δ (ppm) 159.90, 145.36, 138.88, 135.30, 129.94, 123.58, 118.26, 113.87, 112.20, 81.79, 70.58, 39.45, 31.79, 30.57, 25.97, 22.69, 14.11, 11.16. FTIR (KBr, cm^{-1}) 3435, 3064, 2918, 2852, 1733, 1601. Anal. Calcd for $C_{76}H_{86}N_2O_4S_7$. C, 69.36; H, 6.59; N, 2.13. Found C, 69.72; H, 6.73; N, 2.17.

*Poly[4,8-bis(2-(3-(2-hexyldecyloxy)phenyl)-5-thienyl)benzo[1,2-b:4,5-b′]dithiophene-alt-5,6-bis(octyloxy)-4,7-di(thiophen-2-yl) benzo[c][1,2,5]thiadiazole] (**P8**, 59%).* M_n and PDI are 26,000 and 1.3. ^{1}H NMR (300 MHz, $CDCl_3$): δ (ppm) 8.48 (br, 2H), 7.70–7.90 (br, 2H), 7.49 (br, 6H), 7.25–7.30 (br, 4H), 6.89 (br, 4H), 4.14 (br, 4H), 3.91 (br, 4H), 1.81–1.91 (br, 2H), 1.28–1.53 (br, 76H), 0.86 (br, 18H). ^{13}C NMR (600 MHz, $CDCl_3$): δ (ppm) 159.89, 138.75, 135.29, 129.92, 123.25, 118.25, 113.92, 112.18, 102.42, 71.04, 38.03, 31.91, 29.70, 26.88, 14.2. FTIR (KBr, cm^{-1}) 3444, 3064, 2923, 2847, 1729, 1597. Anal. Calcd for $C_{92}H_{118}N_2O_4S_7$. C, 71.73; H, 7.72; N, 1.82. Found. C, 71.43; H, 7.75; N, 2.18.

3. Results and discussion

3.1. Synthesis and characterization

All the monomers and polymers were synthesized according to the route shown in Scheme 2. The *m* and *p*-alkoxy substituted bromophenyl compounds were synthesized by Williamson's aryl ether synthesis from their corresponding bromophenols followed by Stille coupling with 2-tributylstannylthiophene to yield the conjugated APTh (**1**–**4**). These compounds were treated with 4,8-dihydrobenzo[1,2-b:4,5-*b*′]dithiophene-4,8-dione in the presence of *n*-BuLi to give π-conjugated side chain linked BDT derivatives (**5**–**8**) followed by reaction with trimethyltin chloride in the presence of *tert*-BuLi yielded the monomers **D1**–**D4**. Additionally, the monomers **A1** and **A2** were synthesized according to the literature procedures [14,15]. Finally, all the polymers (**P1**–**P8**) were synthesized by microwave-assisted Stille polymerization. All the new monomer structures were confirmed by ^{1}H NMR, ^{13}C NMR, HRMS, FTIR spectroscopies. And the polymers were characterized by ^{1}H NMR, ^{13}C NMR spectroscopy, FTIR spectroscopy, and elemental analysis. The NMR and FTIR spectra of the final compounds are shown in Fig. S1–S8. All the polymers are readily soluble in common organic solvents such as tetrahydrofuran, chloroform, and chlorobenzene. The thermal properties of **P1**–**P8** were measured by thermal gravimetric analysis (TGA) at heating rate of 10 °C/min (Fig. S9) and the data are listed in Table S1. The onset of decomposition temperature (T_d, corresponding to 5% weight loss) of **P1**–**P8** is in the range of 330–430 °C indicating their very high thermal stability. Particularly, the T_d for **P1**–**P4** is higher than that of **P5**–**P8** indicating better close packing arrangement of polymer backbone in the former than that of in the latter series.

3.2. Optical properties

The Uv–Vis absorption spectra of **P1**–**P4** and **P5**–**P8** in chloroform solution and film are shown in Fig. 1a, c and b, d, respectively; it clearly shows that there is a strong influence of nature/position of alkyl chain in APTh with respect to intramolecular non-covalent interactions. All the polymers show dual absorption characteristics; the bands in the lower energy region between 450 and 700 nm are correspond to the intramolecular charge transfer (ICT) interaction between electron rich and deficient units and the bands in the higher energy region between 300 and 400 nm are attributed to the π–π* transition of polymer backbone. The calculated molar extinction coefficients of former series **P1**–**P4** (~6 × 10^4 M^{-1} cm^{-1}) are higher than those of latter series **P5**–**P8** (~5 × 10^4 M^{-1} cm^{-1}). Importantly, the ICT band in **P1**–**P4** has greater absorptivity than their π–π* band. In contrast, the ICT band in **P5**–**P8** has lesser absorptivity than their π–π*. This difference in absorptivity suggests that the former series has more planar backbone than the latter because the extent of ICT interactions mainly depends on the planarity of the backbone. Interestingly, **P1**–**P4** shows a pronounced vibronic shoulder peak between 590 and 620 nm both in solution and film due to the presence of strong intramolecular non-covalent interactions between sulfur atom of thiophene unit and the oxygen atom of carbonyl group; in contrast,

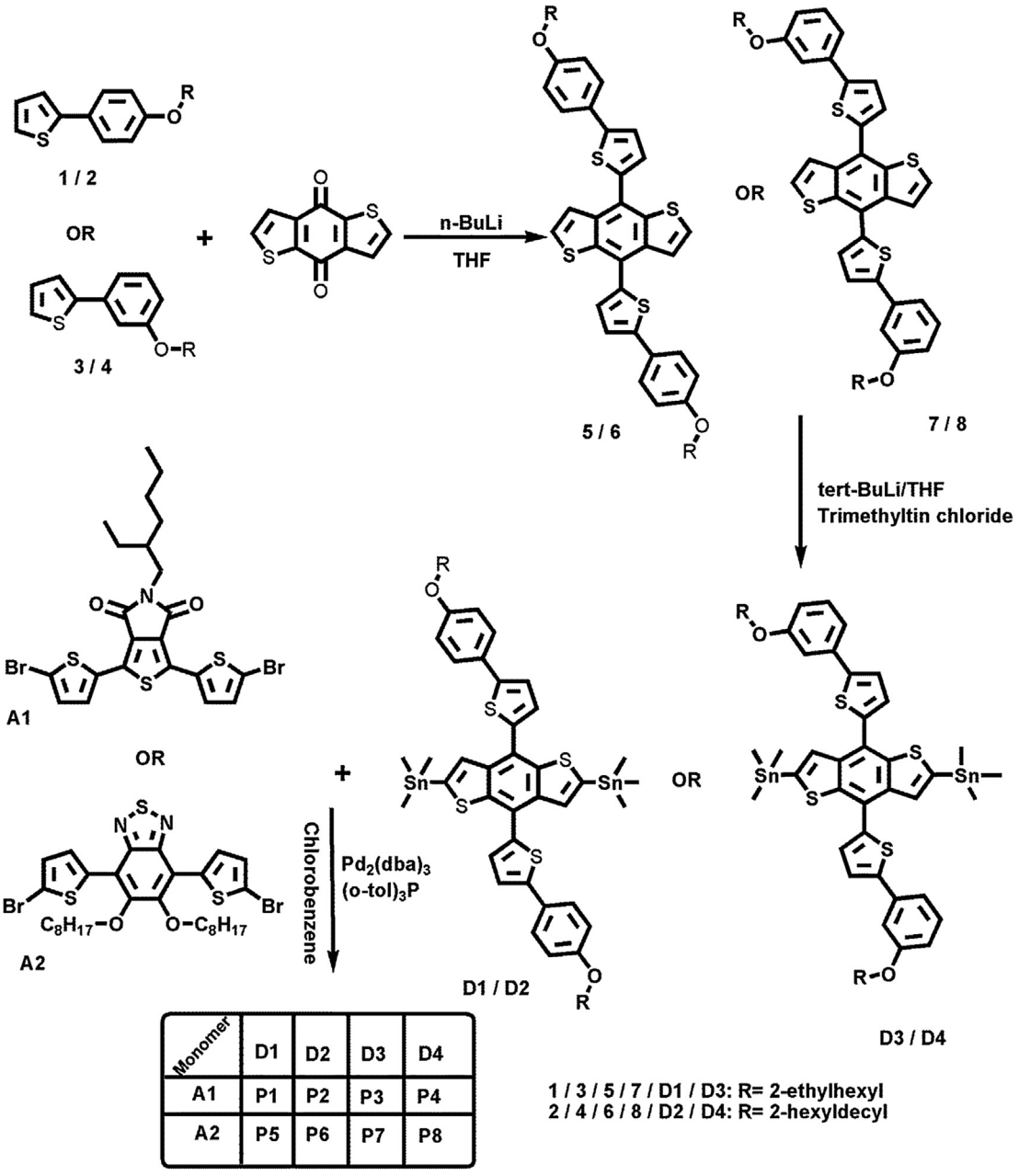

Monomer	D1	D2	D3	D4
A1	P1	P2	P3	P4
A2	P5	P6	P7	P8

Scheme 2. Synthetic route for monomers.

P5–**P8** does not show such a shoulder peak which may be due to the weak intramolecular non-covalent interactions between the alkoxy oxygen and thiophene sulfur. Particularly, vibronic shoulders in **P1**–**P4** are well pronounced in the film state, which further confirms the strong intramolecular non-covalent interactions. Particularly, **P3** shows almost equal relative intensity of the ICT band and the shoulder peak confirms the existence of more planar backbone than their counterparts. This can be further supported by measuring various concentration Uv–Vis absorption spectra of **P1**–**P4** in chloroform. As shown in Fig. S10, the intensity of the shoulder peak is well pronounced upon increasing the concentration of polymer. In contrast, **P5**–**P8** does not show any such pronounced shoulder peaks with similarities. Collectively we conclude that the polymers (**P1**–**P4**) have more planar backbone than the polymers (**P5**–**P8**) due to the presence of strong intramolecular non-covalent interactions in the former than in the latter, which would lead to better charge transporting properties of **P1**–**P4** than that of **P5**–**P8**. In **P1**–**P4**, the ICT band of **P2** (*p*-HDAPTh) appears broader than that of in **P1** (*p*-EHAPTh), in contrast, the **P3** (*m*-EHAPTh) shows broader ICT band than that of in **P4** (*p*-HDAPTh). Particularly, the **P2** and **P3** have a more pronounced vibronic shoulder than that in **P1** and **P4**, a feature which reveals that the position and nature of the alkoxy chains play a key role in the planarization of the polymer backbone. The longer branched alkyl chain in *p*-position (**P2**) and shorter branched alkyl chain in *m*-position (**P3**) show similar absorption patterns with slight red shift of *p*-substituent; the similar absorption patterns also persist in the thin film. Among the *p*-substitution (**P1** and **P2**), the longer alkyl chain (**P2**) shows more red shifted ICT band than the shorter one (**P1**), in contrast, among the *m*-substitution (**P3** and **P4**), the shorter alkyl chain (**P3**) shows more red shifted ICT band than the longer one (**P4**) this might be due to longer alkyl chain in *m*-position leads to more steric hindrance. In the case of **P5**–**P8**, among the *p*-substitution (**P5** and **P6**) the shorter alkyl chain shows red shifted ICT

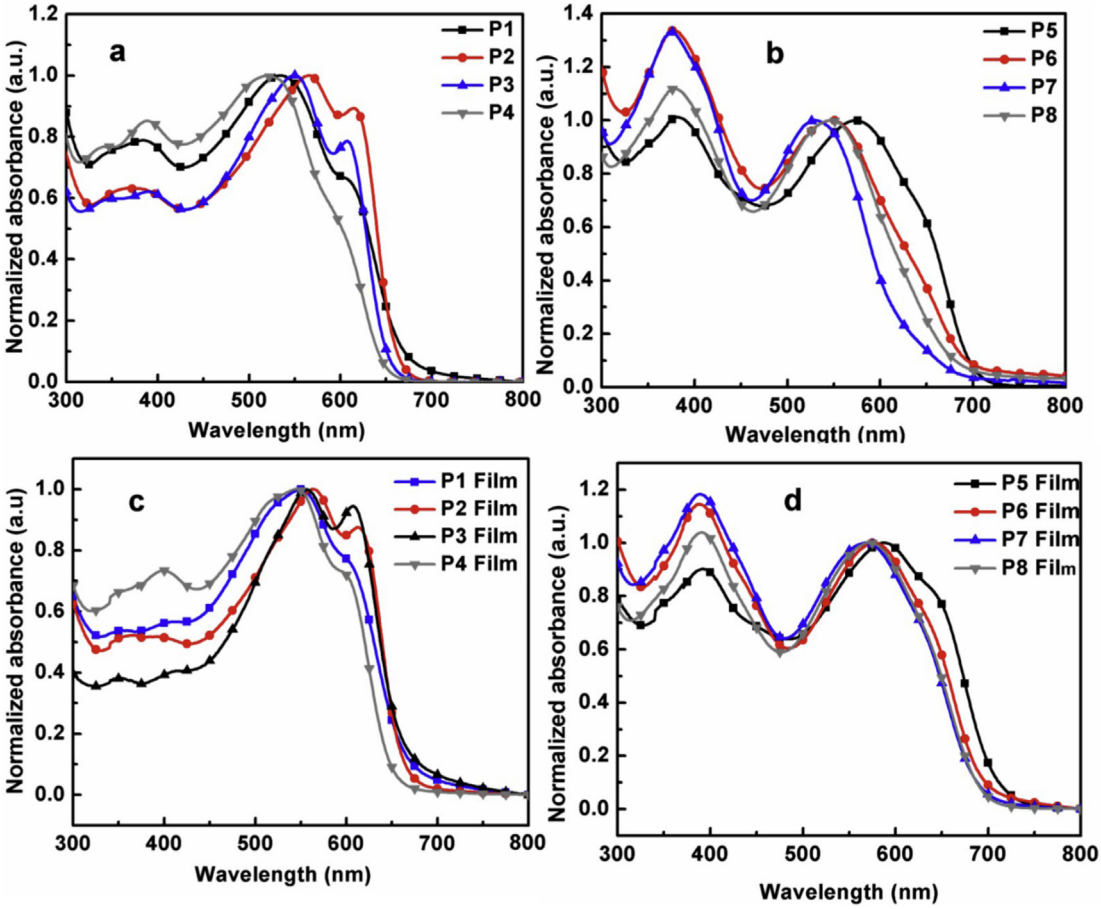

Fig. 1. Uv–Vis absorption spectra of (a) **P1**–**P4** in chloroform solution (b) **P5**–**P8** in chloroform solution (c) **P1**–**P4** film (d) **P5**–**P8** film.

band (**P5**) than the longer one (**P6**), in contrast, among the *m*-substitution, the longer one shows red shifted ICT band (**P8**) than the shorter one (**P7**). Finally, these findings reveal that the position and nature of alkoxy group in APTh have a significant influence on planarization of polymer backbone with respect to their intra-molecular non-covalent interactions in both the series of polymers.

3.3. Electrochemical properties

The electrochemical properties of **P1**–**P8** were measured using cyclic voltammetry (CV) and the corresponding cyclic voltammograms are shown in Fig. S11 and the data are listed in Table 1. The highest occupied molecular orbital (HOMO) energy levels of **P1**–**P8** were determined from their onset of first oxidation potentials. Although, all the polymers show relatively deep HOMO energy level, the **P1**–**P4** possess a deeper HOMO than the **P5**–**P8**, which may enable a high open-circuit voltage (V_{oc}) for the former, since the V_{oc} in mainly depends on the difference between the HOMO of the donor and lowest unoccupied molecular orbital (LUMO) of the acceptor materials. This may be due to the existence of higher electron withdrawing nature of the TPD unit in **P1**–**P4** than that of the BT in **P5**–**P8**. Polymers **P1**–**P8** show the HOMO energy level below the air oxidation threshold limit (5.2 eV), which indicate their air stability. The LUMO energy level of all polymers was calculated from their corresponding optical band gap (E_g^{opt}) and HOMO energy levels. The HOMO and LUMO energy levels of the **P1**–**P8** clearly indicating their good air stability and efficient exciton dissociation at donor/acceptor interfaces, respectively [16].

Table 1
Optical and electrochemical properties of **P1**–**P8**.

Polymer	Solution λ_{max} (nm)[a]	Film λ_{max} (nm)[b]	E_g^{opt} (eV)[c]	HOMO (eV)	LUMO (eV)
P1	526, 601	549, 602	1.81	−5.36	−3.55
P2	564, 615	564, 612	1.82	−5.40	−3.58
P3	548, 607	556, 607	1.76	−5.42	−3.66
P4	516, 583	545, 601	1.84	−5.47	−3.63
P5	574	587	1.68	−5.30	−3.62
P6	546	576	1.68	−5.37	−3.69
P7	531	567	1.74	−5.34	−3.60
P8	546	570	1.76	−5.39	−3.63

[a] Absorption maxima measured from Uv–Vis absorption spectrum in chloroform solution.
[b] Absorption maxima measured from Uv–Vis absorption spectrum in thin film state.
[c] Estimated from the onset of the absorption in thin films ($E_g^{opt} = 1240/\lambda_{onset}$).

3.4. Computational study

Density functional theory (DFT) calculations were carried out using a suite of Gaussian 09 programs to further inspect the electrochemical properties of **P1**–**P8** and analyze the planarity of polymer backbone. Becke's three parameterized Lee-Yang-Parr exchange functional (B3LYP) and 6-31G* basis sets were used [17]. Optimized structures, HOMO and LUMO wave functions of **P1**–**P8** monomers were calculated as shown in Fig. S12. Compared to the LUMOs, the HOMOs are populated widely on the BDT units. As for the LUMOs, orbitals are mainly distributed over TPD or BT units, and show clear charge transfer from the donor to the acceptor. The HOMO energy levels of **P1**–**P4** were calculated to

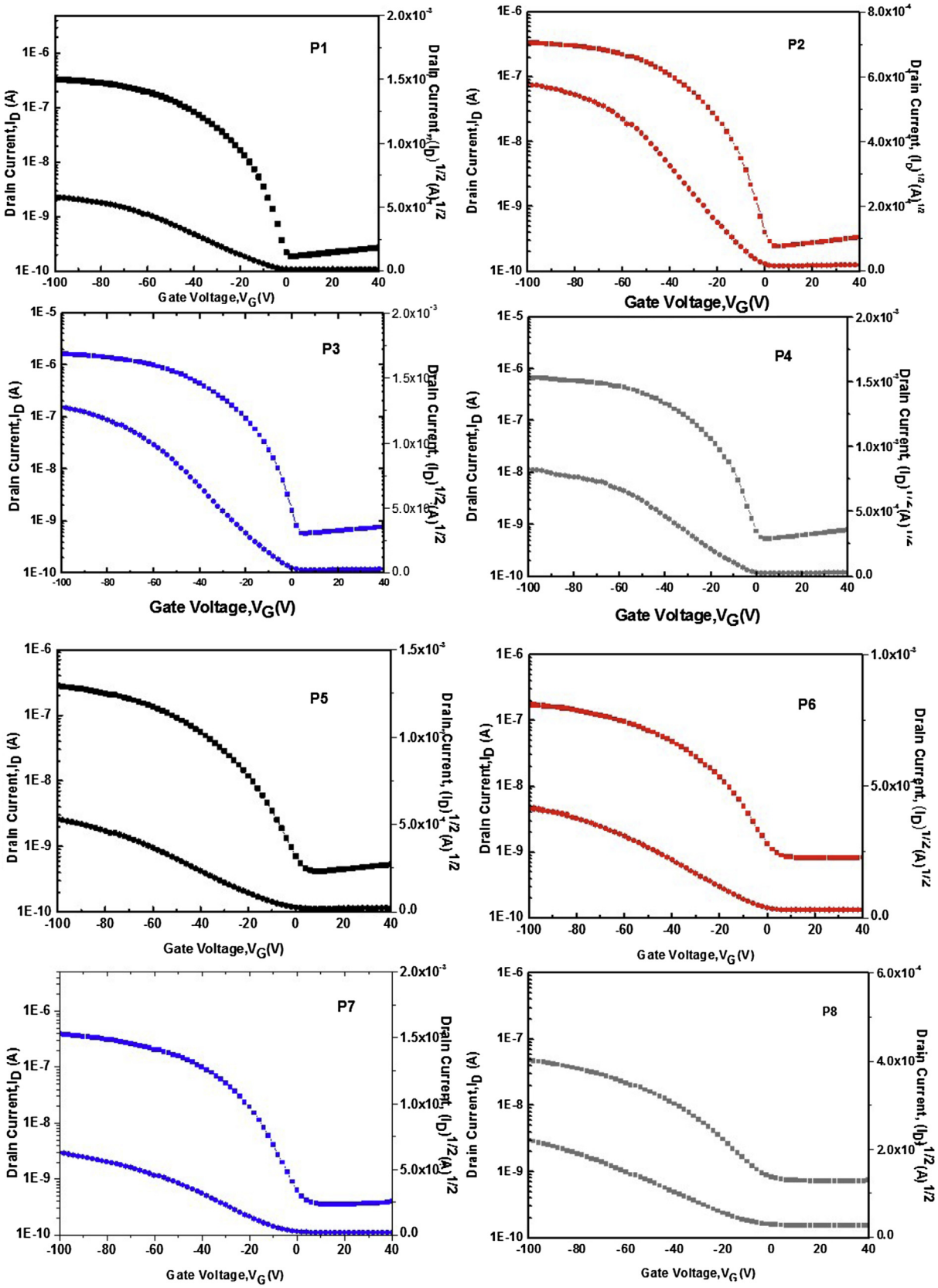

Fig. 2. Transfer characteristic curves of polymer field-effect transistors based on **P1**–**P8**.

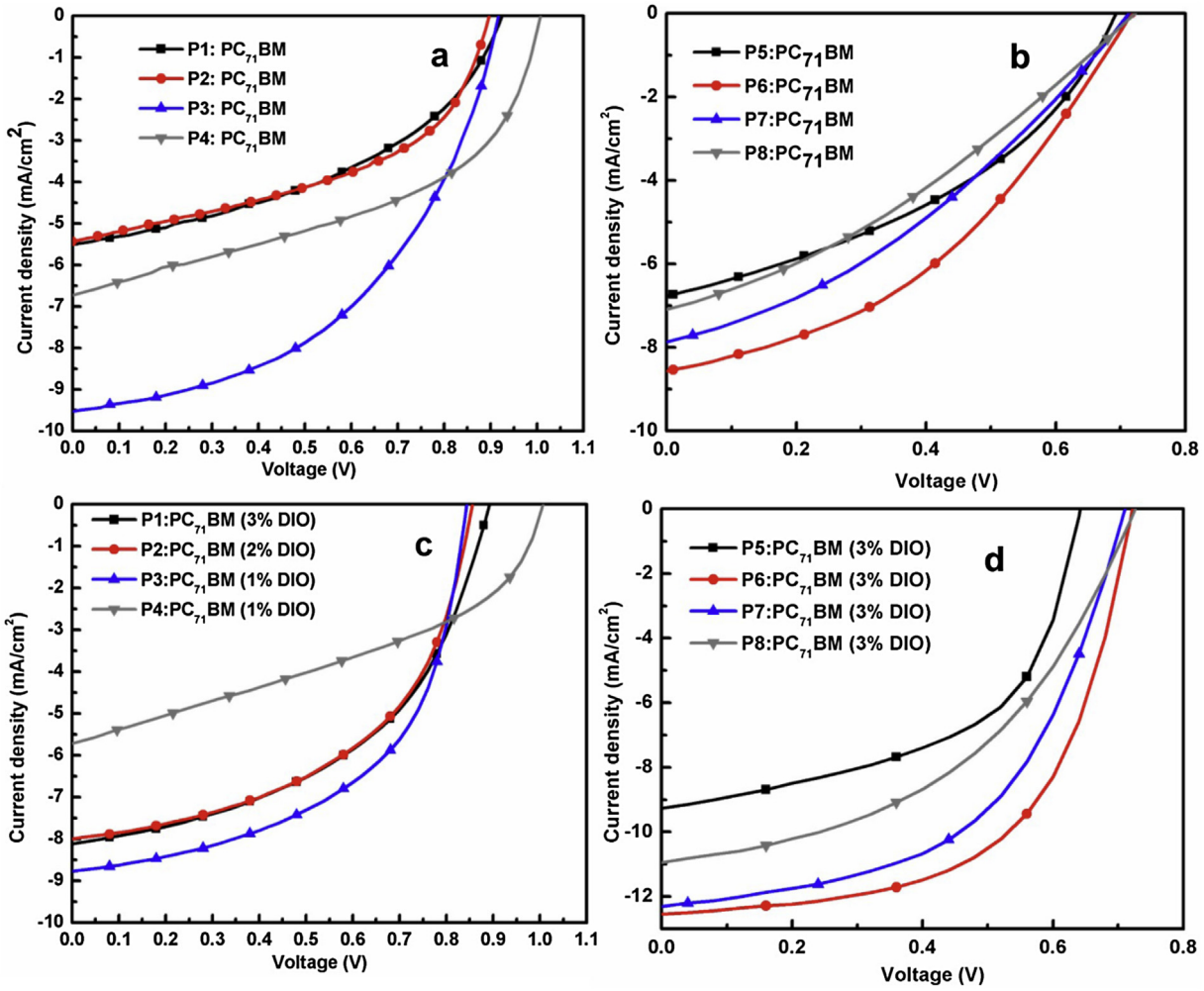

Fig. 3. *J–V* characteristics of **P1**–**P8** without and with DIO.

be −4.89, −4.86, −4.97, and −4.96 eV, respectively, while those of **P5**–**P8** were −4.76, −4.77, −4.80, and −4.81 eV, respectively. These values are in agreement with experimental observations. The planarity of the optimized structures of the repeating units of **P1**–**P8** was also observed through the dihedral angles between the donor and the acceptor units. **P1**–**P4** possess the dihedral angles ranging from 0° to 15°, while **P5**–**P8** ranging from 15° to 30° conform that the polymer **P1**–**P4** have a more planar backbone than that of in **P5**–**P8**. As for electrostatic interactions, calculated Mulliken charge distribution shows an almost equal degree of charge separation between the sulfur atom of thiophene and the oxygen atom of electron deficient units of both the series of polymers. The larger dihedral angle in the latter series might originated from steric repulsions between the lengthy hydrocarbon chain of electron deficient unit BT and the APTh of donor.

3.5. Polymer field effect transistors mobility

The field effect hole mobilities of the **P1**–**P8** were measured in a bottom contact geometry device on a silicon wafer with channel lengths (12 μm) and width (120 μm) under a nitrogen (N_2) atmosphere. All devices were fabricated with polymer thin films as active layer, which were annealed at 140 °C. The transfer characteristics of the devices were shown in Fig. 2 and corresponding data are summarized in Table S2. **P1**–**P8** delivered prominent field-effect hole mobilities, indicating that they possess typical p-type behavior for derived polymer solar cells. Predictably we observed considerable difference in hole mobilities of **P1**–**P8** depending on their side chain nature and position. **P1**–**P4** show higher hole mobilities than **P5**–**P8**. This may be due to the enhanced planarity in **P1**–**P4**. Particularly, **P3** showed the hole mobility in the range of 10^{-3} $cm^2/V \cdot s$. This means that the loss of photocurrent is reduced and thus high photovoltaic performance will be expected for the derived polymer solar cells.

3.6. Photovoltaic properties

To investigate the impact of the nature and position of alkoxy group in the BDT of **P1**–**P8** on their photovoltaic properties, the bulk heterojunction polymer solar cells were fabricated with a

Table 2
Photovoltaic properties of optimized pristine polymer solar cells of **P1**–**P8**.

Polymer	Ratio	J_{sc} (mA/cm^2)	V_{oc} (V)	FF (%)	PCE (%)
P1	1:2	5.48	0.94	43.99	2.27
P2	1:3	5.42	0.89	47.32	2.30
P3	1:2.5	9.50	0.91	48.31	4.19
P4	1:2	6.72	1.00	46.29	3.13
P5	1:2	6.77	0.69	39.96	1.86
P6	1:2	8.46	0.72	40.42	2.45
P7	1:2	7.81	0.71	33.85	1.88
P8	1:2	6.90	0.72	34.24	1.69

Table 3
Photovoltaic properties of optimized polymer solar cells of **P1**–**P8** with DIO.

Polymer	Ratio	J_{sc} (mA/cm^2)	V_{oc} (V)	FF (%)	PCE (%)
P1[c]	1:2	8.15	0.89	49.89	3.61
P2[a]	1:3	7.98	0.85	51.46	3.51
P3[b]	1:2.5	8.89	0.84	53.72	4.03
P4[b]	1:2	5.72	1.00	39.73	2.28
P5[c]	1:2	9.23	0.67	51.57	3.18
P6[c]	1:2	12.73	0.72	57.39	5.26
P7[c]	1:2	12.37	0.72	51.00	4.50
P8[c]	1:2	11.15	0.72	46.82	3.78

[a] 2% DIO.
[b] 1% DIO.
[c] 3% DIO.

configuration of ITO/PEDOT:PSS/polymer:$PC_{71}BM$/LiF/Al and measured under the illumination of AM 1.5G illumination (100 mW/cm^2). The active layer of the device was spin-coated from the chlorobenzene solution of the corresponding polymer and $PC_{71}BM$ blend. Several device processing conditions such as polymer to $PC_{71}BM$ ratio, film thickness, and external additive concentration were carefully optimized to get best device performance. Fig. 3a and b shows the current density–voltage (J–V) curves of optimized devices of a pristine blend of **P1**–**P4** and **P5**–**P8**, respectively, and the data are summarized in Table 2. Interestingly, **P3** shows higher short-circuit current density (J_{sc}) of 9.50 mA/cm^2 than their counterparts (**P1**, **P2** and **P4**) although the absorption coverage of **P1**–**P4** are almost similar, which can be realized by the existence of a highly planar backbone in **P3**. Whereas **P5**–**P8** exhibited J_{sc} in the range of 6.77–8.46 mA/cm^2 with a maximum of 8.46 mA/cm^2 for **P6**, which is higher than that of **P5**. Although **P5** has broader absorption coverage than that of **P6**, the polymer **P6** is showing higher J_{sc} may be due to the morphological mismatches. Considering the V_{oc} of the polymers, **P1**–**P4** show higher V_{oc} than that of **P5**–**P8** due to the deeper HOMO of the former. The V_{oc} values are very similar in **P1**–**P4** and in **P5**–**P8** with a maximum of 1 V and 0.72 V for **P4** and **P6/P8**, respectively. It suggests that the V_{oc} value of pristine blend films mainly correlate with the energy gap between the HOMO of the donor polymer and LUMO of the $PC_{71}BM$ in the active layer rather than the morphology between them. Additionally, **P1**–**P4** also show higher fill factor (FF) values than that of **P5**–**P8** which might be due to the high hole mobility and better morphological nature, hence, **P1**–**P4** show higher power conversion efficiency (PCE) than the **P5**–**P8**. Particularly, **P3** shows a PCE of 4.19% for pristine blend film due to the higher J_{sc}, V_{oc}, and FF values than those of its counterparts. This can be realized by very high planar backbone of **P3** that leads to nanoscale phase separation in the active layer along with the very high V_{oc} of 0.91 V. Among **P5**–**P8**, the polymer **P6** displays a better photovoltaic performance with a maximum PCE of 2.45%. Finally, it is believed that *m*-EHAPTh (**P3**) unit is highly suitable for enhancing the planarity of backbone among **P1**–**P4**. It is well known that upon addition of a certain amount of solvent additive to the active layer

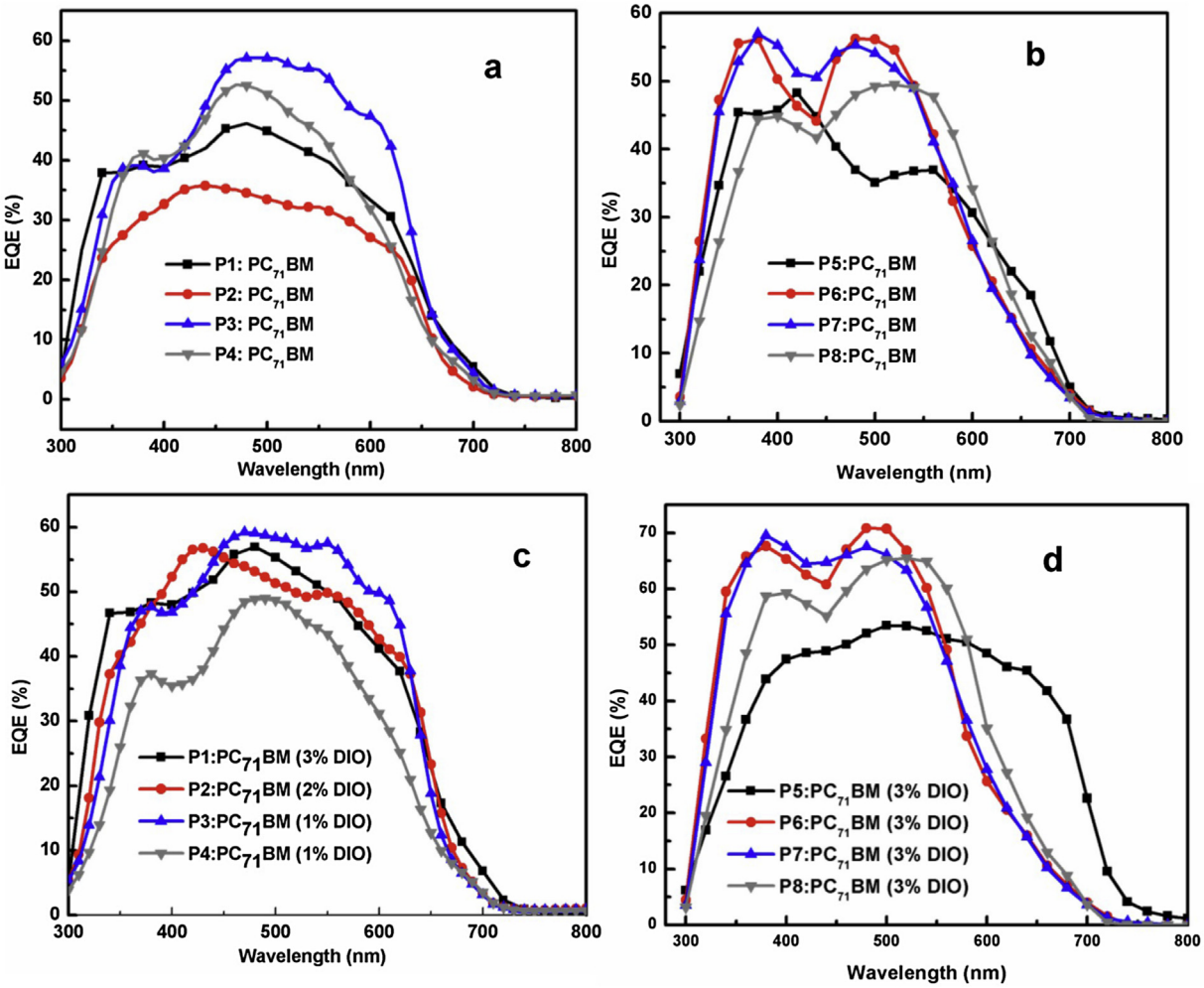

Fig. 4. EQE spectra of **P1**–**P8** without and with DIO.

of bulk heterojunction polymer solar cells, the photovoltaic properties are improved due to the enhancement of phase separation in morphology. In this regard, the optimized photovoltaic properties of all the polymers were further analyzed in the presence of DIO.

The photovoltaic properties of **P1**–**P4** and **P5**–**P8** based devices in the presence of DIO are listed in Table 3. Upon addition of DIO to the active layers of two series of polymers, latter series (**P5**–**P8**) showed improved device performance compared to the former series (**P1**–**P4**) This is due to the fact that the DIO could able to improve the active layer morphology in case of **P5**–**P8** based devices whereas, in **P1**–**P4** based devices, it would have destroyed the already existed good phase separation in the active layer. In addition to this, the influence of DIO is also depends on the nature and position of the alkoxy group in π-conjugated side chain linker of BDT in **P5**–**P8**. Especially the J_{sc} and PCE of **P6** is increased from 8.46 mA/cm^2 and 2.45% to 12.73 mA/cm^2 and 5.26%, respectively. However in the case of **P1**–**P4** based devices, upon addition of DIO to the active layers the photovoltaic performance of **P1**, **P2** is slightly increased and **P3**, **P4** is decreased.

Fig. 4a and b shows the external quantum efficiency (EQE) curves of **P1**–**P4** and **P5**–**P8**, optimized devices without DIO. All devices show a broad response in the range of 300–700 nm, which are consistent with absorption spectra of the corresponding polymers. Even though all devices could absorb the photons between 300 and 700 nm, the percentage of EQE varies significantly between the polymers. This is due to the nature of the donor and acceptor materials and the morphology between them in the active layer. Upon considering the EQE of **P1**–**P4**, the polymer **P3** shows very broad EQE with a maximum of ~60% consistent with the higher J_{sc} that leads to higher PCE. Upon addition of DIO to the active layer of **P1**–**P4**, the EQE value of **P1** and **P2** is increased, but for **P3** and **P4** is decreased as shown in Fig. 4c due to the morphological mismatching in the active layer, which is consistent with the photovoltaic performances. In case of **P5**–**P8**, the EQE is increased for all the polymers as shown in Fig. 4d upon addition of DIO which may be due to the improved phase separated morphological nature than their pristine counterparts. The J_{sc} values calculated from integration of the EQE spectra were well matched with J_{sc} obtained from the *J*–*V* measurements.

3.7. Morphological studies

To analyze further the difference between the photovoltaic properties of polymers, the morphology of the active layer of the corresponding polymers was investigated using tapping-mode atomic force microscopy (AFM). Fig. 5 shows the representative

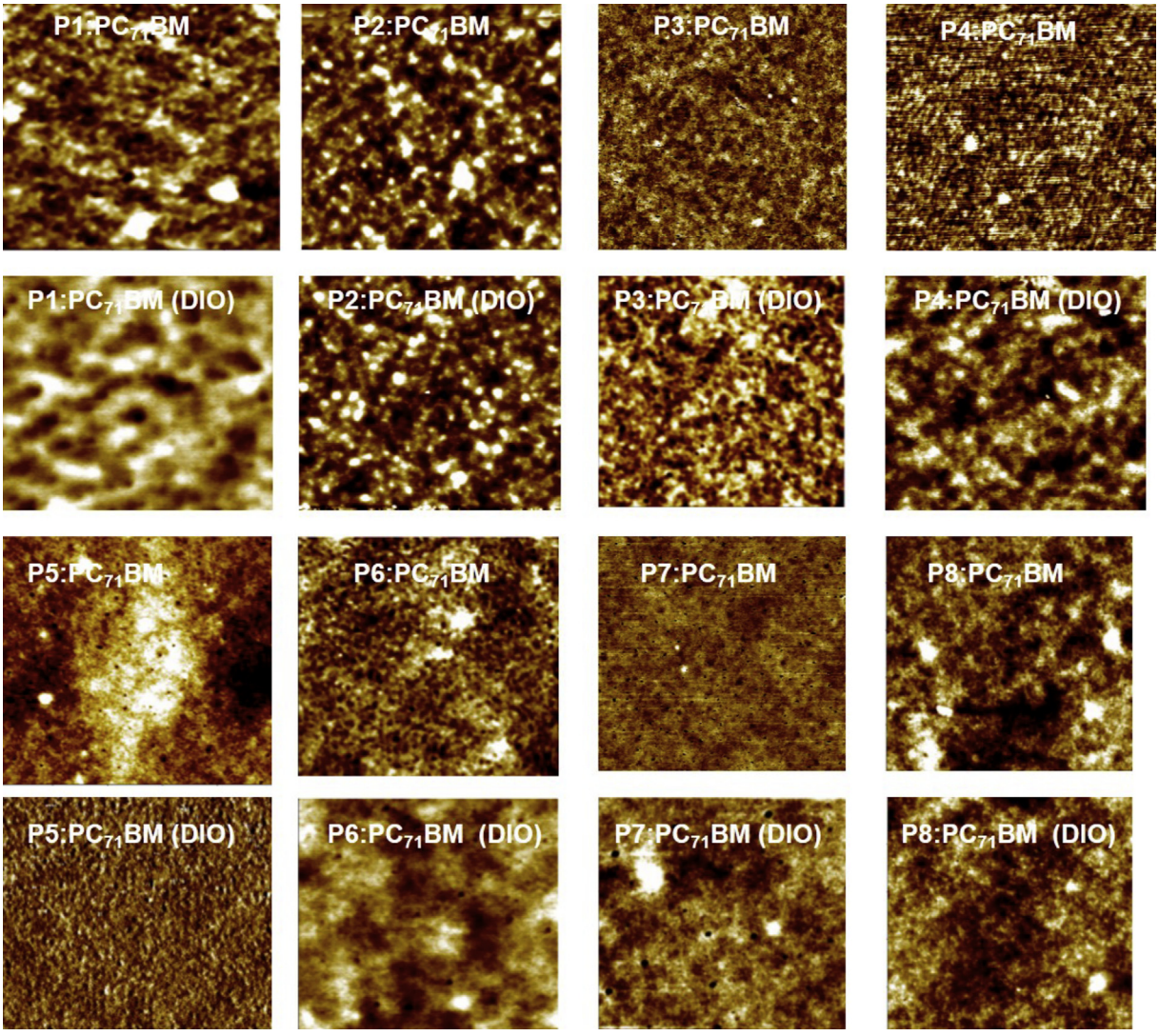

Fig. 5. AFM images of active layers based **P1**–**P8** without and with DIO.

AFM images of optimized blend films of **P1**–**P8**. In the case of **P1**–**P4**, the active layer of **P3** shows well organized nanoscale morphology better than that of **P1**, **P2**, and **P4** and is consistent with the superior photovoltaic properties. This is caused by the well-organized planar backbone of **P3**. Upon addition of DIO to the active layer of **P1**–**P4**, the surface roughness is decreased for **P1** and **P2** and increased for **P3** and **P4**. This is consistent with the higher device performance of **P1** and **P2** and lesser performance of **P3** and **P4** in the presence of DIO than their pristine counterparts, respectively. Very interestingly, the AFM images of pristine active layers of **P3** and **P4** shows well organized nano structures, a feature which is consistent with the superior photovoltaic properties in neat blends. Upon addition of DIO, the root mean square (RMS) roughness of the image is increased due to the disturbance of the present nano structure. This indicates that the well-organized polymer backbone of **P3** and **P4** are completely disturbed by DIO, which leads to reduce the photovoltaic performance. On the contrary, in the case of **P5**–**P8**, the surface roughness of all the polymers is decreased upon addition of DIO. Thus, **P5**–**P8** displays superior photovoltaic performance than their pristine counterparts. This indicates that the DIO modulates the morphology of the active layer for better charge transportation that leads to improved photovoltaic performance. Due to this reason the PCE of **P6** and **P7** is increased from 2.45 to 1.88% to 5.26 and 4.50%, respectively.

4. Conclusions

We successfully designed and synthesized two series of low band gap polymers (**P1**–**P4** and **P5**–**P8**) containing APTh linked BDT based electron rich and A1/A2 based electron deficient units to explore the effect of intramolecular non-covalent interactions with respect to position and nature of alkoxy groups in APTh. Between the two series of polymers, the **P1**–**P4** show the ICT band with higher absorptivity than their π–π^* band and well defined shoulder peaks that indicate the existence of a more planar backbone in **P1**–**P4** than that in **P5**–**P8**; this is due to the fact that the presence of strong intramolecular non-covalent interactions in **P1**–**P4**. The higher polymer filed effect transistor mobilities of **P1**–**P4** compared to **P5**–**P8** due to the presence of a more planar backbone in **P1**–**P4**. Resultantly, **P1**–**P4** based pristine devices showed superior photovoltaic properties than the **P5**–**P8** with the maximum PCE of 4.19% for **P3**. Upon addition of DIO to the active layer of all the optimized devices, the photovoltaic performance of **P1** and **P2** are increased and decreased for **P3** and **P4** due to the disruption of already existed well interpenetrating nanoscale morphology; but in the case of **P5**–**P8**, the DIO drastically improved the photovoltaic performances, especially the PCE of **P6** and **P7** is elevated from 2.45 to 1.88% to 5.26 and 4.50%, respectively. From the above results we concluded that change in intramolecular non-covalent interactions by modulating the side chain nature and position significantly changes in the planarity of backbone, optoelectronic properties, polymer field effect transistor mobilities and also photovoltaic properties of **P1**–**P8**. The foregoing results open a new simple strategy to modulate optoelectronic properties of polymers changing the position and nature of alkoxy group of APTh with respect to their intramolecular non-covalent interactions. We believe that this article will give a deep insight about the alkoxy side chain nature and position in APTh of polymer backbone and how it influences the bulk properties of resulted polymers.

Acknowledgments

This work was supported by grant fund from the National Research Foundation (NRF) (2011-0028320) and the Pioneer Research Center Program through the NRF (2013M3C1A3065522) by the Ministry of Science, ICT & Future Planning (MSIP) of Korea.

Appendix A. Supplementary data

Supplementary data related to this article can be found at http://dx.doi.org/10.1016/j.dyepig.2015.07.032.

References

[1] Cheng YJ, Yang SH, Hsu CS. Synthesis of conjugated polymers for organic solar cell applications. Chem Rev 2009;109:5868–923.
[2] Ye L, Zhang S, Huo L, Zhang M, Hou J. Molecular design toward highly efficient photovoltaic polymers based on two-dimensional conjugated benzodithiophene. Acc Chem Res 2014;47:1595–603.
[3] Piliego C, Holcombe TW, Douglas JD, Woo CH, Beaujuge PM, Frechet JMJ. Synthetic control of structural order in N-alkylthieno[3,4-c]pyrrole-4,6-dione-based polymers for efficient solar cells. J Am Chem Soc 2010;132:7595–7.
[4] Yum S, An TK, Wang X, Lee W, Uddin MA, Kim YJ, et al. Benzotriazole-containing planar conjugated polymers with noncovalent conformational locks for thermally stable and efficient polymer field-effect transistors. Chem Mater 2014;26:2147–54.
[5] Rieger R, Beckmann D, Mavrinskiy A, Kastler M, Mullen K. Backbone curvature in polythiophenes. Chem Mater 2010;22:5314–8.
[6] Guo X, Baumgarten M, Mullen K. Designing-conjugated polymers for optoelectronics. Prog Polym Sci 2013;38:1832–908.
[7] Zuo G, Li Z, Zhang M, Guo X, Wu Y, Zhang S, et al. Influence of the backbone conformation of conjugated polymers on morphology. Polym Chem 2014;5:1976–81.
[8] Cheng YJ, Ho YJ, Chen CH, Kao WS, Wu CE, Hsu SL, et al. Photophysical and photovoltaic properties of conjugated polymers containing fused donor-acceptor dithienopyrrolobenzothiadiazole and dithienopyrroloquinoxaline arenes. Macromolecules 2012;45:2690–8.
[9] Qi J, Zhou X, Yang D, Qiao W, Ma D, Wang ZY. Optimization of solubility film morphology and photodetector performance by molecular side-chain engineering of low-bandgap thienothiadiazole-based polymers. Adv Funct Mater 2014;24:7605–12.
[10] Guo X, Zhou N, Lou SJ, Hennek JW, Oritz RP, Butler MR, et al. Bithiopheneimide-dithienosilole/dithienogermole copolymers for efficient solar cells: information from structure-property-device performance correlations and comparison to thieno[3,4-c]pyrrole-4,6dione analogues. J Am Chem Soc 2012;134:18427–39.
[11] Nguyen TL, Choi H, Ko SJ, Uddin MA, Walker B, Yum S, et al. Semicrystalline photovoltaic polymers with efficiency exceeding 9% in a ~300 nm thick conventional single-cell device. Energy Environ Sci 2014;7:3040–51.
[12] Mei J, Bao Z. Side chain engineering in solution processable conjugated polymers. Chem Mater 2014;26:604–15.
[13] Kranthiraja K, Gunasekar K, Cho W, Song M, Park YG, Lee JY, et al. Alkoxyphenylthiophene linked benzodithiophene based medium band gap polymers for organic photovoltaics: efficiency improvement upon methanol treatment depends on the planarity of backbone. Macromolecules 2014;47:7060–9.
[14] Najari A, Beaupre S, Berrouard P, Zou Y, Pouliot JR, Perusse CL, et al. Synthesis and characterization of new thieno[3,4-c]pyrrole-4,6-dione derivatives for photovoltaic applications. Adv Funct Mater 2011;21:718–28.
[15] Ding P, Chu CC, Liu B, Peng B, Zou Y, He Y, et al. A high mobility low-bandgap copolymer for efficient solar cells. Macromol Chem Phys 2010;211:2555–61.
[16] Li Y, Xu B, Li H, Cheng W, Xue L, Chen F, et al. Molecular engineering of copolymers with donor-acceptor structure for bulk heterojunction photovoltaic cells toward high photovoltaic performance. J Phys Chem C 2011;115:2386–97.
[17] Frisch MJ, Trucks GW, Schlegel HB, Scuseria GE, Robb MA, Cheeseman JR, et al. Gaussian 09, revision A.01. Wallingford, CT, USA: Gaussian, Inc.; 2009.